Applied Catalysis B: Environmental 91 (2009) 663–669

Contents lists available at ScienceDirect

Applied Catalysis B: Environmental

journal homepage: www.elsevier.com/locate/apcatb

Electrocatalytic activity of Pt nanoparticles deposited on porous TiO_2 supports toward methanol oxidation

Chung-Shou Chen, Fu-Ming Pan *

Department of Materials Science and Engineering, National Chiao-Tung University, 1001 Ta Hsueh Road, Hsinchu 30010, Taiwan, ROC

ARTICLE INFO

Article history:
Received 21 April 2009
Received in revised form 1 July 2009
Accepted 12 July 2009
Available online 18 July 2009

Keywords:
Porous TiO_2
Platinum
Hydrothermal method
CO oxidation
Methanol electro-oxidation

ABSTRACT

Porous TiO_2 thin films were prepared on the Si substrate by hydrothermal method, and used as the Pt electrocatalyst support for methanol oxidation study. Well-dispersed Pt nanoparticles with a particle size of 5–7 nm were pulse-electrodeposited on the porous TiO_2 support, which was mainly composed of the anatase phase after an annealing at 600 °C in vacuum. Cyclic voltammetry (CV) and CO stripping measurements showed that the Pt/TiO_2 electrode had a high electrocatalytic activity toward methanol oxidation and an excellent CO tolerance. The excellent electrocatalytic performance of the electrode is ascribed to the synergistic effect of Pt nanoparticles and the porous TiO_2 support on CO oxidation. The strong electronic interaction between Pt and the TiO_2 support may modify CO chemisorption properties on Pt nanoparticles, thereby facilitating CO oxidation on Pt nanoparticles via the bifunctional mechanism and thus improving the electrocatalytic activity of the Pt catalyst toward methanol oxidation.

1. Introduction

Direct methanol fuel cell (DMFC) has received extensive studies in the past decade because of the great application potential for a renewable power source. DMFCs can be operated at low temperatures, have a high energy density and a long life and are lightweight with a simple system design. Although DMFCs possess many merits as a power source, practical commercialization still faces several fundamental materials challenges. As far as the methanol oxidation reaction (MOR) is concerned, major challenges receiving particular attention are a higher electrocatalytic activity with a minimized Pt catalyst loading and a better resistance against the CO poisoning effect. The widely adopted method to improve the electrocatalytic mass activity of the precious Pt catalyst toward MOR is to disperse Pt nanoparticles on the catalyst support of large surface area [1–7]. On the other hand, to improve the CO tolerance, considerable studies used Pt-based binary or ternary alloys as the catalyst, in particular Pt–Ru, to enhance CO electro-oxidation via the bifunctional mechanism and/or the so-called electronic effect [8–15]. Metal oxides, such as CeO_2, SnO_2 and RuO_2, can also effectively improve the CO tolerance of the Pt catalyst when used as a promoter or the catalyst support based on a similar principle [16–20].

TiO_2 is one of the most important transition metal oxides with a wide range of industrial applications. TiO_2 has intriguing photocatalytic properties and excellent chemical stability in both acidic and alkaline solutions, and has long been used as a catalyst or support in photo-electrochemical systems. Many recent studies on titania for DMFC applications prepared titania supports of high surface area for the Pt catalyst loading and found that the oxide supports could significantly enhance the electrocatalytic activity and the CO tolerance of the Pt catalyst [21–26]. The better electrocatalytic properties of Pt/TiO_2 electrodes are usually attributed to the bifunctional mechanism and a strong metal–support interaction between the TiO_2 and the Pt catalyst [27,28]. In the study, we used hydrothermal method to prepare porous TiO_2 thin film as a catalyst support and pulse-electrodeposited Pt nanoparticles on the porous thin film vacuum-annealed at 600 °C. Electrochemical study shows that the annealed porous TiO_2 support can greatly improve the CO tolerance of the Pt catalyst, thus leading to a better electrocatalytic activity toward MOR.

2. Experimental

2.1. Preparation of the porous TiO_2 support

To prepare the porous titania support, a Ti thin film of 100 nm thick was first deposited on a p-type 6-in. Si wafer of low resistivity (0.002 Ω cm) by electron beam evaporation (e-beam) deposition. The Ti thin film coated silicon wafer was then immersed in the aqueous solution of 10 M NaOH at 80 °C for 25 min, followed by a rinse with 0.1 M HNO_3. Before the Pt nanoparticle deposition on the porous TiO_2 support, the as-synthesized thin film was annealed

* Corresponding author. Tel.: +886 3 5131322; fax: +886 3 5724727.
E-mail address: fmpan@faculty.nctu.edu.tw (F.-M. Pan).

0926-3373/$ – see front matter © 2009 Elsevier B.V. All rights reserved.
doi:10.1016/j.apcatb.2009.07.008

in vacuum (10^{-7} Torr) at various temperatures to improve the electrical conductivity of the porous support.

2.2. Pulse electrodeposition of Pt nanoparticles

Pt nanoparticles were electrodeposited on the TiO_2 support in the aqueous solution of 0.001 M H_2PtCl_6 (200 ml)/0.33 M HCl (2 ml) at room temperature by galvanostatic pulse plating in a three-electrode cell system with a saturated calomel reference electrode (SCE). The vacuum-annealed porous TiO_2 support was used as the working electrode and a Pt plate as the counter electrode. The particle size and dispersion of Pt nanoparticles can be controlled by tuning the pulse height of the applied current and the pulse duration. The time durations for the high current pulse (4 mA) and the low current pulse (−20 mA) were 2 and 1 ms, respectively. A total of 3000 pulse cycles were performed to deposit Pt nanoparticles on the porous TiO_2 support. For comparison, Pt particles of larger size were also electrodeposited on a blanket TiO_2 surface, which was prepared by annealing a Ti thin film 10 nm thick on the Si substrate in oxygen ambient at 600 °C for 5 min, followed by vacuum anneal at 600 °C for 1 h. A Pt island film and a blanket-Pt thin film of 5 nm thickness were also deposited by pulse electrodeposition and e-beam deposition, respectively, on a metallic Ti thin film, which was e-beam deposited on the Si wafer. The mass loading of the Pt catalyst on the support was determined by inductively coupled plasma mass spectroscopy (Thermo X Series II).

2.3. Electrochemical measurements and materials characterizations

Electrochemical measurements were conducted at room temperatures in the same electrochemical cells as that used for the Pt electrodeposition. The working electrode was the Pt/TiO_2 electrode. All aqueous solutions were prepared with low resistance DI water (∼18 MΩ) produced by an ultrapure water purification system. The cyclic voltammetry (CV) measurement of methanol electro-oxidation was carried out in the mixture solution of 1 M H_2SO_4 + 1 M CH_3OH within the potential range of −0.2 to 0.9 V (vs. SCE) with a scan rate of 20 mV s^{-1}. Prior to the CV measurement, the electrolyte was purged with pure N_2 gas for 20 min to remove excess dissolved oxygen. The CO stripping measurement was conducted in a 0.5 M H_2SO_4 solution within the potential range of −0.2 to 0.9 V with a scan rate of 20 mV s^{-1}. The CO adsorption on the Pt catalyst was performed by flowing a 10% CO/N_2 gas mixture in the 0.5 M H_2SO_4 aqueous solution at 100 mV for 30 min. Before the CO stripping measurement, the solution was purged with pure N_2 gas for 10 min to remove CO remaining in the solution. The chronoamperometric measurement for CH_3OH oxidation was carried out in the solution of 1 M H_2SO_4 + 1 M CH_3OH at 0.5 V for 3600 s.

Surface morphology of the samples was examined by scanning electron microscopy (SEM, JEOL JSM-6700F). X-ray diffractometry (XRD, PANalytical X'Pert Pro) with the Cu Kα source was used to study the crystallinity of the porous TiO_2 support vacuum-annealed at various temperatures. The microstructure and particle size distribution of Pt nanoparticles were analyzed by transmission electron microscopy (TEM, JEOL JEM-3000F). The TEM specimens were prepared by scratching off the Pt/TiO_2 layer from the Si substrate with a pair of dissecting forceps in the presence of a small drop of ethanol, and then put onto a holly-copper grid and dried in air at the room temperature.

3. Results and discussion

3.1. Material characterizations

Fig. 1(a) and (b) shows the plane-view SEM images of the as-prepared hydrothermally synthesized TiO_2 thin film and the porous film annealed at 600 °C for 3 h (thereafter denoted as TiO_2-3 h), respectively. The thin film had a carpet-like morphology with collapsed thin sheets on the surface. According to the cross-sectional SEM image shown in Fig. 1(c), the hydrothermalized thin film had a two-layer structure with the carpet-like layer on the top and an ill-compacted granular layer on the bottom. The top and bottom layers were ∼260 nm and ∼65 nm thick, respectively. It is not clear to us at the present time why the two different microstructure layers were formed during the one-step hydrothermal treatment. The top layer was virtually of a porous structure, which was constructed by mutually overlaying collapsed sheets. A careful examination from the cross-sectional SEM image of Fig. 1(c) reveals that the pore walls were composed of nanosized grains connecting with one another, and with a wall thickness roughly the diameter of a grain, which was ∼15–25 nm. Compared to the blanket Ti thin film before hydrothermalization, the porous morphology of the hydrothermal TiO_2 thin film provided a much larger surface area for the Pt catalyst loading. Fig. 1(d) shows the plane-view SEM image of the TiO_2-3 h thin film after the pulse electrodeposition of Pt catalyst (thereafter denoted as Pt/TiO_2-3 h). Because the electrodeposited Pt nanoparticles were very small in size and well dispersed on the TiO_2 pore structure as will be shown by TEM images, they are hardly observed in the SEM image. Also shown in Fig. 1 are the SEM images of electrodeposited Pt particles on the blanket TiO_2 surface (Fig. 1(e)), Pt islands on the Ti thin film (Fig. 1(f)) and the e-beam deposited Pt thin film (Fig. 1(g)). Pt particles on the blanket TiO_2 thin film (thereafter denoted as Pt/TiO_2-tf) had a relatively uniform size distribution around ∼15–20 nm and well dispersed on the surface. For Pt islands deposited on the Ti surface (denoted as Pt/Ti), islands with sizes mostly larger than 300 nm covered nearly the whole Ti substrate surface. On the other hand, the e-beam deposited Pt thin film completely capped the Ti substrate and will be denoted as the blanket-Pt electrode. These three samples will be used for comparison when we discuss later about the electrocatalytic activity of the Pt/TiO_2-3 h electrode.

TiO_2 is an n-type semiconductor, and the electrical conductivity of TiO_2 increases with the concentration of donor-like oxygen vacancies [29]. The conductivity may increase by more than four orders of magnitude when the oxygen/Ti stoichiometry ratio varies from 2.0 to 1.7 [30]. The electrical conductivity of a TiO_2 film can be greatly improved by a reducing treatment, e.g. thermal anneal under vacuum conditions [31]. Because the as-synthesized porous TiO_2 thin film had a relatively high electrical resistivity, Pt electrodeposition on the porous TiO_2 support was barely possible. To increase the conductivity of the TiO_2 support, the as-prepared porous thin film was thermally annealed in a vacuum of 1×10^{-7} Torr. Fig. 2 shows XRD spectra of the TiO_2 thin film annealed at various temperatures. For the as-prepared TiO_2 thin film (curve a), the two diffraction peaks situated at 25.4° and 48° are due to the anatase (1 0 1) and (2 0 0) lattice planes, respectively. The peak at 55.5° may result from the overlap of the two adjacent peaks due to the anatase (2 1 1) and (1 0 5) lattice planes. The three diffraction peaks were weak and broad, indicating poor crystallinity and/or finite size effect. At temperatures below 500 °C, the intensity of the three peaks decreased with the annealing temperature. This was more apparent for the (2 0 0) plane, which was nearly undetectable at 400 °C. As the annealing temperature reached 500 °C, the three peaks showed a reverse trend in the intensity variation, i.e. the peak intensity increased with the temperature. For the sample annealed at 600 °C for 1 h, the anatase (1 0 1) peak became narrower with an obvious increase in the peak height. When the annealing time increased to 3 h, the anatase (1 0 1) peak grew much shaper and stronger, and the anatase (2 0 0) peak became clearly detectable with a narrow width. The XRD analysis suggested that the thermal annealing at

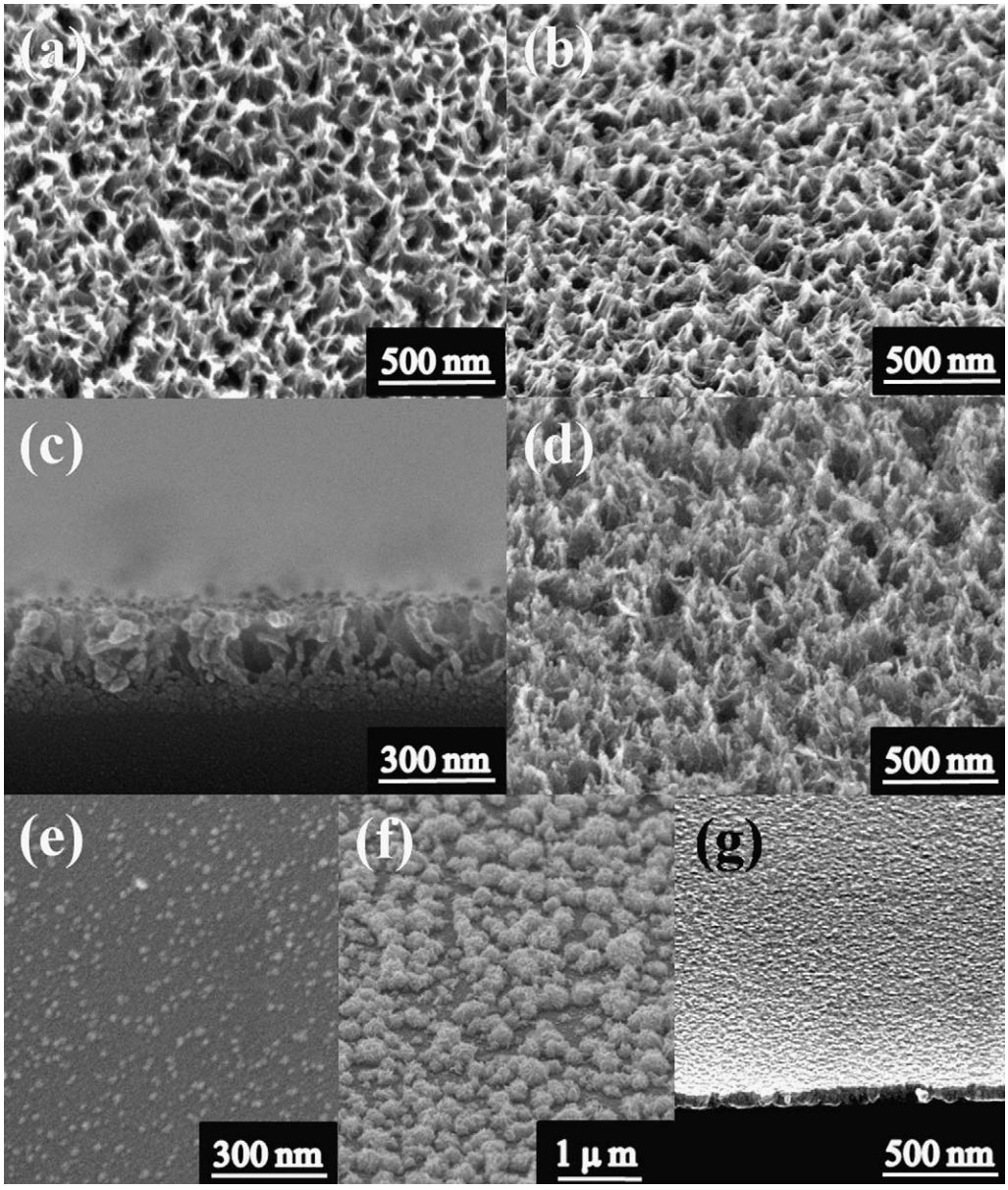

Fig. 1. SEM images for (a) the as-prepared porous TiO_2 thin film, (b) porous TiO_2-3 h thin film, (c) cross-section of the porous TiO_2-3 h thin film, (d) Pt nanoparticles deposited on the porous TiO_2-3 h thin film, (e) Pt particles deposited on the blanket TiO_2 thin film, (f) Pt islands on the Ti substrate, and (g) blanket-Pt thin film on the Ti substrate.

600 °C in vacuum improved the crystallinity of the anatase phase and made the porous TiO_2 thin film preferentially (1 0 1) oriented. The better crystallinity of the anatase phase seemed to play an important role in improving the electrical conductivity of the porous TiO_2 thin film. Pt nanoparticles could be easily electrodeposited on the TiO_2 thin film annealed at temperatures at 600 °C, and electrochemical measurements could be performed without difficulty. On the contrary, no electrochemical operation could be effectively conducted for samples annealed at temperatures below 500 °C.

Fig. 3(a) shows the bright-field TEM image of electrodeposited Pt nanoparticles on the Pt/TiO_2-3 h electrode. Nanoparticles with a dark contrast are the electrodeposited Pt catalyst, as revealed by the lattice fringe of the Pt(1 1 1) plane (~0.23 nm) in the high resolution TEM (HRTEM) image shown in Fig. 3(b). Also indexed in Fig. 3(b) is the TiO_2 anatase (1 0 1) plane (~0.35 nm). According to the TEM image, Pt nanoparticles with a size distribution ranging from 4 to 7 nm adhered over the TiO_2 grain cluster. The small size and well dispersion of the Pt nanoparticles on the porous TiO_2 support can create a large Pt surface, thereby resulting in a large electrochemically active surface area (ESA).

3.2. Electrochemical measurements

The ESA of the Pt catalyst was evaluated by the CO stripping CV measurement. Fig. 4 shows the CO stripping CV curves of the Pt/TiO_2-3 h, Pt/TiO_2-tf, Pt/Ti and blanket-Pt electrodes. The ESA was determined by the following equation:

$$\mathrm{ESA} = \frac{Q_{\mathrm{CO}}}{[\mathrm{Pt}] \times 0.484} \quad (1)$$

where Q_{CO} (mC cm^{-2}) is the total charge involved in the electro-oxidation reaction of CO adspecies, [Pt] is the mass loading per unit area of the Pt catalyst on the electrode and 0.484 represents the oxidation charge for a monolayer of CO adsorbed on a smooth Pt surface. Q_{CO} was calculated by integrating the area of the CO oxidation peak in the first CO stripping cycle. The measured Pt

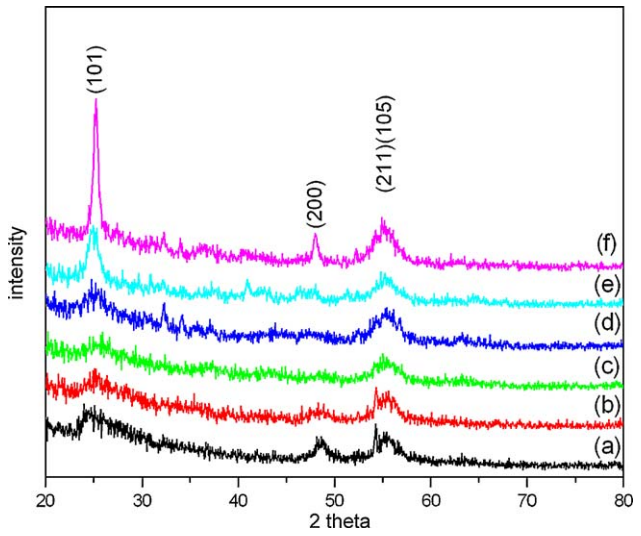

Fig. 2. X-ray diffraction spectra of the porous TiO_2 thin film annealed at various temperatures for 1 h: (a) as-prepared, (b) 300 °C, (c) 400 °C, (d) 500 °C, (e) 600 °C and (f) 600 °C for 3 h.

loadings of the Pt/TiO_2-3 h, Pt/TiO_2-tf, Pt/Ti and blanket-Pt electrodes are 0.01697, 0.01095, 0.03774 and 0.06279 mg/cm^2, respectively. The ESA of the Pt/TiO_2-3 h electrode was thereby calculated to be 172.9 m^2 g^{-1}, which was much higher than that of Pt/TiO_2-tf, Pt/Ti and blanket-Pt electrodes (114.6, 26.3 and 57.1 m^2 g^{-1}, respectively). The much larger ESA of the Pt/TiO_2-3 h electrode can significantly improve electrocatalytic activity toward MOR compared to the other three electrodes.

Fig. 5 shows the MOR CV curves of the Pt/TiO_2-3 h, Pt/TiO_2-tf, Pt/Ti and blanket-Pt electrodes in the aqueous solution of 1 M CH_3OH and 1 M H_2SO_4. Because of the larger ESA, the Pt/TiO_2-3 h electrode has a much higher MOR current density than the other three electrodes. The methanol electro-oxidation peak of the Pt/TiO_2-3 h electrode had the maximum around 0.58 V with the onset potential at ~0.28 V, which is herein defined as the MOR potential at which the current density reaches 0.1 mA/cm^2. For the Pt/TiO_2-tf, Pt/Ti and blanket-Pt electrodes, the CV curves had the anodic peak potential at 0.59, 0.62 and 0.65 V with the onset potential at 0.40, 0.41 and 0.48 V, respectively. For MOR on the Pt catalyst in an acidic electrolyte, the anodic peaks in the forward scan and in the reverse scan of a CV measurement are associated with methanol oxidation and the removal of incompletely oxidized carbonaceous species, respectively. During the reverse scan, residual linear Pt=C=O adspecies can be oxidized by Pt–OH_{ads} in the acidic electrolyte within the potential range where the reverse anodic peak develops [32]. Therefore, the ratio of the anodic peak current density in the forward scan (I_f) to that in the reverse scan (I_b), (I_f/I_b), is a useful index for evaluating the CO tolerance of a MOR catalyst [33]. The I_f/I_b ratios of the Pt/TiO_2-3 h, Pt/TiO_2-tf, Pt/Ti and blanket-Pt electrodes were about 1.44, 1.21, 1.06 and 1.1, respectively. The larger I_f/I_b ratio of the Pt/TiO_2-3 h electrode suggests that the electrode had a higher resistance against CO poisoning in MOR. The improved CO tolerance of the Pt/TiO_2-3 h electrode can play a key role in reducing the MOR overpotential leading to the smaller onset and peak potentials observed in the CV measurement.

The CO stripping CV curves shown in Fig. 4 provide the direct evidence that the Pt/TiO_2-3 h electrode had a much better CO tolerance in the acidic solution compared to the Pt/TiO_2-tf, Pt-Ti and blanket-Pt electrodes. The CO stripping CV curve of the Pt/TiO_2-3 h electrode exhibited two distinct peaks at 0.42 and 0.47 V vs. SCE with a gradual rising feature within the potential range between 0.2 and 0.4 V. For CO adspecies on Pt, two electro-

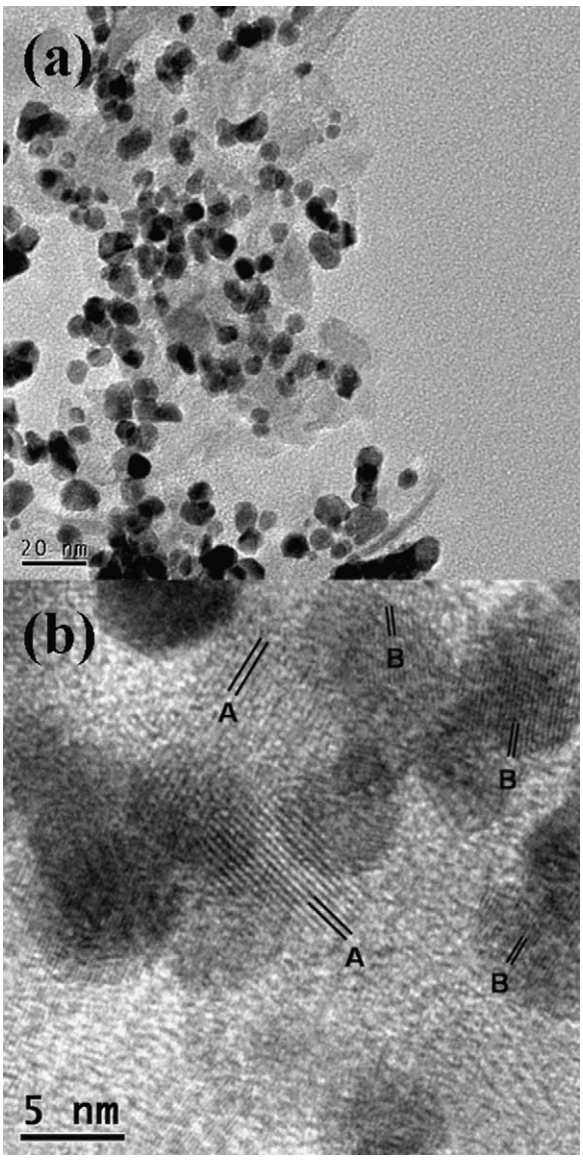

Fig. 3. (a) TEM and (b) HRTEM images of Pt nanoparticles on the TiO_2-3 h support. The lattice fringes labeled by A and B are due to the anatase (1 0 1) and the Pt(1 1 1) lattice planes, respectively.

oxidation peaks are usually detected within the potential range between 0.7 and 1.0 V vs. RHE [34–36]. The low potential peak was ascribed to CO electro-oxidation on the (1 1 0) plane or edge sites on the (1 1 1) plane, and the high potential peak was due to CO electro-oxidation on the (1 1 1) plane [36]. Thus the doublet peak measured in the study may be assigned to CO electro-oxidation on such surface sites as well. According to the TEM image of Fig. 3(a), many of Pt nanoparticles on the anatase support clearly show various polyhedron shapes. Nanocrystals with a polyhedral shape are usually enclosed mainly by {1 0 0} and {1 1 1} facets [37]. Therefore the (1 0 0) surface plane must also take part in the electrocatalytic reaction of CO oxidation. The electrocatalytic activity of Pt toward CO oxidation varies with the Pt surface orientation, increasing in the order Pt(1 1 1) < Pt(1 1 0) < Pt(1 0 0) [38]. As a result, CO electro-oxidation on the Pt(1 0 0) surface will take place at a lower potential than on the (1 1 1) and (1 1 0) surfaces. It is likely that the CV signal due to CO electro-oxidation on (1 0 0) surface sites contributes to the rising feature on the low potential side of the doublet peak. Compared with the Pt/TiO_2-3 h electrode, the Pt/TiO_2-tf electrode shows a featureless broad peak

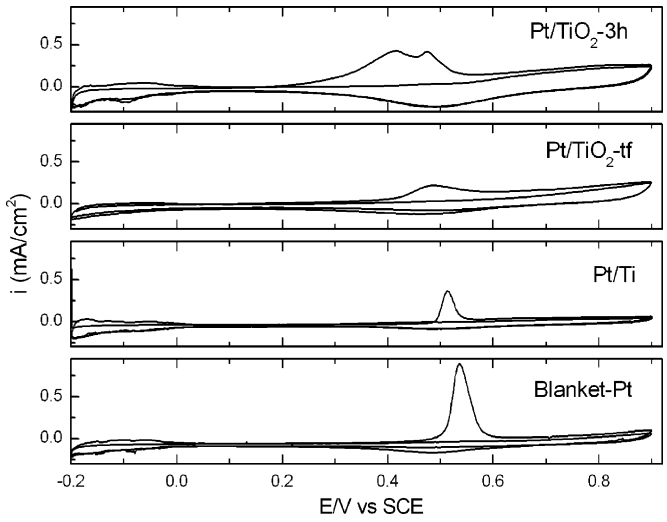

Fig. 4. CO stripping cyclic voltammograms of the Pt/TiO_2-3 h, Pt/TiO_2-tf, Pt/Ti and blanket-Pt electrodes in a CO saturated 0.5 M H_2SO_4 solution. The scan rate was 20 mV s^{-1}.

with the peak maximum at 0.49 V. Because both the Pt/TiO_2-tf and the Pt/TiO_2-3 h electrodes have Pt catalysts electrodeposited on the TiO_2 surface, the difference in the CO electro-oxidation behavior between these two electrodes is very likely to result from differences in the particle size and shape of the Pt electrocatalysts and, possibly, the morphology of the TiO_2 supports. The Pt/Ti and the blanket-Pt film electrodes exhibit a single CO electro-oxidation peak at a much higher potential with the peak maximum at 0.52 and 0.54 V, respectively. The single CO stripping peak indicates that the Pt catalyst on both electrodes had a surface crystallography greatly different from nanosized Pt particles on the porous TiO_2 support.

One other possible explanation for the slowly rising CV curve feature with the very low onset potential (~0.29 V vs. SCE) is the repulsive interaction between CO adspecies on the Pt nanoparticles, which could weaken the bond strength of CO adspecies with the Pt lattice sites. The heat of adsorption of CO on Pt(*h k l*) surfaces is strongly coverage-dependent [39], and defects on nanoparticles have a significant impact on the local CO coverage [40]. As the coverage of the CO adspecies decreased due to the continuous CO oxidation process during the CV scan, the adsorption heat of CO adspecies on the Pt surface progressively increased because of the gradual decrease of the repulsive interaction. The CO oxidation potential thus shifted accordingly to the higher regime, leading to the appearance of the gradual rising feature within the potential range of 0.2–0.4 V.

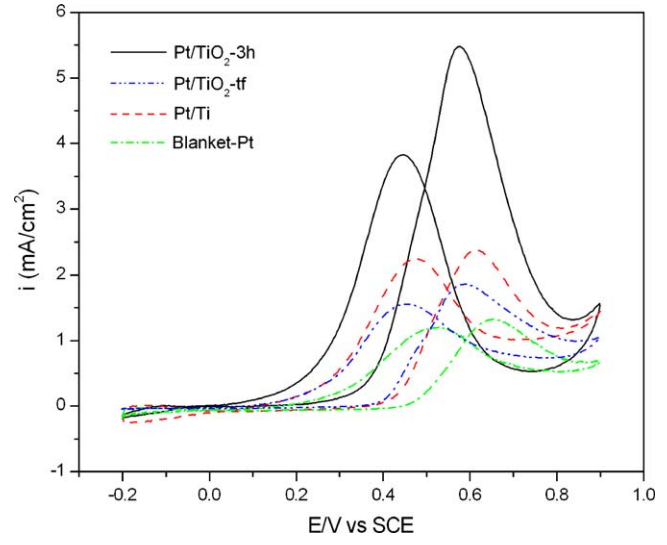

Fig. 5. Cyclic voltammograms of methanol electro-oxidation for the Pt/TiO_2-3 h, Pt/TiO_2-tf, Pt/Ti and blanket-Pt electrodes in the 1 M CH_3OH + 1 M H_2SO_4 solution. The scan rate was 20 mV s^{-1}.

The much better electrocatalytic performance of the Pt/TiO_2-3 h electrode compared to the other three electrodes, such as the lower onset potential for both the CO electro-oxidation and MOR, can be ascribed to the synergistic effect of the nanosized Pt catalyst and the TiO_2 support. There are two widely accepted models accounting for the enhancement of electrocatalytic activity of the supported Pt catalyst: the bifunctional mechanism [41–44] and the electronic effect (or ligand effect) [27,28,45–47]. TiO_2 can not only promote CO tolerance via the bifunctional mechanism, but may also modify the electronic structure of Pt nanoparticles in terms of the electronic effect. The bifunctional mechanism is widely used to describe how hydroxyl surface groups can oxidize and remove adjacent CO adspecies from the Pt catalyst surface, thus avoiding CO poisoning. For TiO_2 supported Pt nanoparticles, CO adspecies bound on the periphery of Pt nanoparticles can be readily oxidized via the bifunctional mechanism by neighboring Ti–OH groups, which may result from dissociative adsorption of water molecules on the TiO_2 surface. Theoretical studies have shown that spontaneous dissociative adsorption of water molecules effectively proceeds on the (0 0 1) surface of titania, whereas molecular adsorption prevails on the (1 0 1) surface [48–50]. Because the crystallite shape of anatase TiO_2 was a truncated bipyramid exposing both the (1 0 1) and (0 0 1) surfaces [50], it is likely that the porous TiO_2 support may provide a large quantity of (0 0 1) surface planes when the size of anatase grains on the support is close to the nanometer scale. Thus dissociative H_2O adsorption on the (0 0 1) anatase surface will create abundant Ti–OH surface groups on the TiO_2 support in the electrolyte, thereby promoting CO electro-oxidation on the Pt catalyst via the bifunctional mechanism. CO electro-oxidation via the bifunctional mechanism is likely more pronounced on the periphery of Pt nanoparticles due to the immediate contact of CO adspecies with Ti–OH groups surrounding the Pt nanoparticles.

An additional likely explanation for the better CO tolerance of the Pt/TiO_2-3 h electrode is that chemisorption properties of noble metals can be significantly altered by interactions with the TiO_2 surface [27,28,51]. The strong hypo–hyper-d-electron interaction between the TiO_2 support and Pt nanoparticles may greatly modify the electronic structure of Pt atoms at the interface. As a consequence, the catalytic activity of CO oxidation on Pt surface may be improved if modification of the adsorption strength of CO adspecies can accordingly reduce the activation barrier for the CO oxidation reaction. This is particularly true for Pt surface atoms situated in the peripheral region of Pt nanoparticles, which may be only a few atoms in width, because they directly bond to the TiO_2 support and act as the catalytic surface sites. The peripheral Pt atoms are more liable to the electronic effect than those surface atoms sitting apart from the periphery, and therefore should exhibit distinct electrocatalytic activity toward CO oxidation. As the size of Pt nanoparticles become smaller, the number of peripheral Pt sites will increase resulting in an electrocatalytic activity more characteristic for CO oxidation on the peripheral sites. On the other hand, Pt particles with a larger particle size have a lower electrocatalytic activity possibly due to the less effective electronic effect [52]. Moreover, diffusivity of adspecies on Pt particles subject to the strong electronic interaction with the support may be significantly modified. Hepel et al. recently reported that the CO surface diffusivity on the Pt nanoparticle can be improved due to the weakened CO adsorption strength on Pt

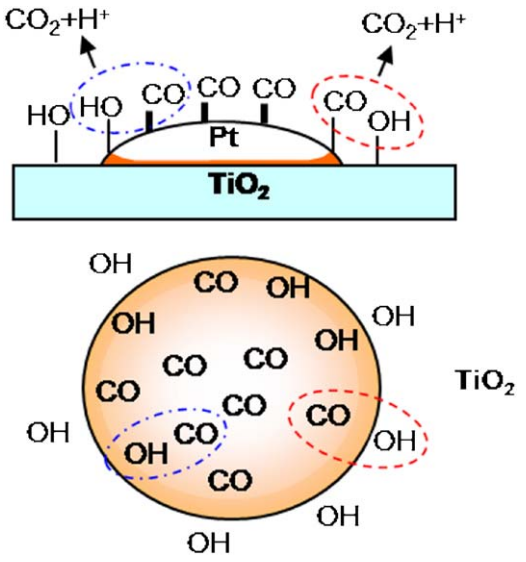

Fig. 6. Schematic diagram illustrating the synergistic effect of the Pt nanoparticle and the anatase TiO_2 support on CO oxidation on the Pt nanoparticle.

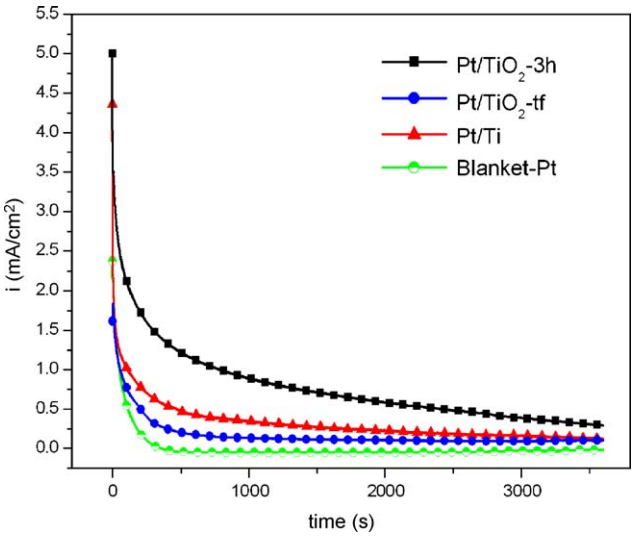

Fig. 7. Chronoamperometry curves of the Pt/TiO_2-3 h, Pt/TiO_2-tf, Pt/Ti and blanket-Pt electrodes in the solution of 1 M CH_3OH + 1 M H_2SO_4 at room temperature for 1 h. The oxidation potential was kept at 0.5 V vs. SCE.

nanoparticles supported on TiO_2 nanotubes [53]. Because of the nanoscaled size (<5 nm) of Pt catalyst particles on the porous TiO_2 support, CO and/or OH adspecies can readily diffuse over the Pt nanoparticle, thereby facilitating a better efficiency of CO oxidation via the Langmuir–Hinshelwood reaction mechanism, in which adsorbed reactants diffuse, collide and form products on the surface. The above discussion can explain the difference in the MOR electroactivity between the Pt/TiO_2-3 h and the Pt/TiO_2-tf electrodes.

For better understanding of the above described synergistic effect of the Pt nanoparticles and the TiO_2 support, Fig. 6 schematically illustrates the likely reaction steps of CO oxidation on the Pt nanoparticle, which can be described by the following reaction equations:

$$TiO_2 + H_2O \rightarrow TiO_2{-}OH + H^+ + e^-, \quad (2)$$

$$TiO_2{-}OH + Pt{-}CO \rightarrow CO_2 + Pt + TiO_2 + H^+ + e^-, \quad (3)$$

$$Pt + H_2O \rightarrow Pt{-}OH + H^+ + e^-, \quad (4)$$

$$Pt{-}CO + Pt{-}OH \rightarrow 2Pt + CO_2 + H^+ + e^-. \quad (5)$$

The Pt catalyst is illustrated in the figure as a hemispherical particle for clarity. The interface area in the Pt nanoparticle is shaded to indicate the strong electronic interaction between Pt and the TiO_2 support. Dissociative adsorption of water molecules on the TiO_2 support creates TiO_2–OH surface groups. TiO_2–OH groups adjacent to Pt nanoparticles may readily oxidize CO groups bonded on the peripheral Pt atoms, of which the electronic structure is greatly modified by the TiO_2 support. Once a free Pt site is created by the CO oxidation reaction, an OH surface group can then be adsorbed on the free Pt site by dissociative adsorption of an H_2O molecule or OH adspecies migration from other Pt sites or the TiO_2 surface. The OH surface group can then oxidize a CO group sitting on a neighboring Pt site, creating two free Pt sites, and the CO oxidation reaction will continue if any Pt–CO group is present on the reaction front. Because the reaction rate increases with the density of available Pt sites, the electrocatalytic activity toward CO oxidation will become more and more thriving till the coverage of CO adspecies is significantly diminished.

Fig. 7 shows the chronoamperograms of the electroactivity of the Pt/TiO_2-3 h, Pt/TiO_2-tf, Pt/Ti and blanket-Pt electrodes at the oxidation potential of 0.5 V in the 1 M CH_3OH/1 M H_2SO_4 aqueous solution at 25 °C. All the four electrodes showed a decay in the MOR electroactivity with time. This is most obvious for the blanket-Pt, which had a rapid drop in the current density to 0.04 mA/cm^2 within the first 500 s. On the other hand, the Pt/TiO_2-3 h electrode shows a moderate current density decay and has a much higher electrocatalytic activity as compared to the other three electrodes. The Pt/TiO_2-3 h electrode still keeps a current density of ~0.3 mA/cm^2 after 1 h of methanol oxidation in the acidic solution. The higher electroactivity stability of the Pt/TiO_2-3 h electrode may be attributed to the large ESA and the enhanced CO tolerance. CO adspecies could be effectively oxidized and removed from the Pt catalyst nanoparticles so that the catalytic oxidation of methanol proceeded more efficiently on the Pt/TiO_2-3 h electrode

4. Conclusions

The study prepared porous TiO_2 thin film on the Si substrate by hydrothermal method for the use of the Pt catalyst support for MOR electroactivity study. The porous TiO_2 support was mainly composed of anatase phase after vacuum annealing at 600 °C and showed an electrical conductivity good for Pt electroplating and electrochemical measurement. Because of the porous structure of the TiO_2 support and well-dispersed Pt nanoparticles, the Pt/TiO_2-3 h electrode had a much larger ESA compared to the Pt/TiO_2-tf, Pt/Ti and the blanket-Pt electrodes. MOR CV and CO stripping measurements indicated that the Pt/TiO_2-3 h electrode had a high electrocatalytic activity toward MOR and a very good CO tolerance. We ascribe the good CO tolerance to the synergistic effect of Pt nanoparticles and the porous TiO_2 support. The nanosized scale of the Pt catalyst allows easy access of CO adspecies by hydroxyl surface groups on the TiO_2 surface, thereby CO electro-oxidation prevails around the peripheral area of Pt nanoparticles via bifunctional mechanism. Moreover, the strong electronic interaction between the Pt nanoparticle and the TiO_2 substrate might weaken the chemisorption strength of CO adspecies on the Pt catalyst, and thus enhance CO electro-oxidation activity.

Acknowledgment

This work was supported by the National Science Council of R.O.C. under Contract No. NSC96-2221-E009109-MY3.

References

[1] G. Che, B.B. Lakshmi, E.R. Fisher, C.R. Martin, Nature 393 (1998) 346.
[2] M.L. Anderson, R.M. Stroud, D.R. Rolison, Nano Lett. 2 (2002) 235.
[3] S.H. Joo, S.J. Choi, I. Oh, J. Kwak, Z. Liu, O. Terasaki, R. Ryoo, Nature 412 (2001) 169.
[4] B. Rajesh, K.R. Thampia, J.-M. Bonard, A.J. McEvoy, N. Xanthopoulos, H.J. Mathieu, B. Viswanathan, J. Power Sources 133 (2004) 155.
[5] W. Li, X. Wang, Z. Chen, M. Waje, Y. Yan, J. Phys. Chem. B 110 (2006) 15353.
[6] J.N. Tiwari, T.M. Chen, F.M. Pan, K.L. Lin, J. Power Sources 182 (2008) 510.
[7] T. Maiyalagan, Appl. Catal. B 80 (2008) 286.
[8] T. Frelink, W. Visscher, J.A.R. van Veen, Surf. Sci. 335 (1995) 353.
[9] C. Lu, C. Rice, R.I. Masel, P.K. Babu, P. Waszczuk, H.S. Kim, E. Oldfield, A. Wieckowski, J. Phys. Chem. B 106 (2002) 9581.
[10] J.-M. Léger, S. Rousseau, C. Coutanceau, F. Hahn, C. Lamy, Electrochim. Acta 50 (2005) 5118.
[11] P. Waszczuk, G.-Q. Lu, A. Wieckowski, C. Lub, C. Rice, R.I. Masel, Electrochim. Acta 47 (2002) 3637.
[12] F. Maillard, G.-Q. Lu, A. Wieckowski, U. Stimming, J. Phys. Chem. B 109 (2005) 16230.
[13] G.Y. Zhao, G.L. Xu, D.J. Guo, H. Li, H.L. Li, J. Power Sources 162 (2006) 492.
[14] M.C. Tsai, T.K. Yeh, C.H. Tsai, Electrochem. Commun. 145 (2006) 1445.
[15] E. Antolini, Appl. Catal. B 74 (2007) 337.
[16] C. Xua, Z. Tian, P. Shen, S.P. Jiang, Electrochim. Acta 53 (2008) 2610.
[17] J. Wang, S. Yu, J. Xi, L. Chen, W. Zhu, X. Qiua, Electrochem. Solid-State Lett. 10 (2007) B114.
[18] L.X. Yang, C. Bock, B. MacDougall, J. Park, J. Appl. Electrochem. 34 (2004) 427.
[19] M.S. Saha, R. Li, M. Cai, X. Sun, Electrochem. Solid-State Lett. 10 (2007) B130.
[20] Y.J. Gu, W.T. Wong, J. Electrochem. Soc. 153 (9) (2006) A1714.
[21] H. Song, X. Qiu, D. Guo, F. Li, J. Power Sources 178 (2008) 97.
[22] M. Gustavsson, H. Ekström, P. Hanarp, L. Eurenius, G. Lindbergh, E. Olsson, B. Kasemo, J. Power Sources 163 (2007) 671.
[23] B.E. Hayden, D.V. Malevich, D. Pletcher, Electrochem. Commun. 3 (2001) 390.
[24] B.E. Hayden, D. Pletcher, J.P. Suchsland, L.J. Williams, Phys. Chem. Chem. Phys. 11 (2009) 1564.
[25] Q.Z. Jiang, X. Wu, M. Shen, Z.F. Ma, X.Y. Zhu, Catal. Lett. 124 (2008) 434.
[26] T. Maiyalagan, B. Viswanathan, U.V. Varadaraju, J. Nanosci. Nanotechnol. 6 (2006) 2067.
[27] J.R. Croy, S. Mostafa, J. Liu, Y. Sohn, H. Heinrich, B.R. Cuenya, Catal. Lett. 119 (2007) 209.
[28] S.G. Neophytides, K. Murase, S. Zafeiratos, G. Papakonstantinou, F.E. Paloukis, N.V. Krstajic, M.M. Jaksic, J. Phys. Chem. B 110 (2006) 3030.
[29] B. Huber, H. Gnaser, C. Ziegler, Surf. Sci. 566 (2004) 419.
[30] S. Guerin, B.E. Hayden, D. Pletcher, M.E. Rendall, J.P. Suchsland, L.J. Williams, J. Combinat. Chem. 8 (2006) 791.
[31] A. Rothschild, Y. Komem, A. Levakov, N. Ashkenasy, Y. Shapira, Appl. Phys. Lett. 82 (2003) 574.
[32] J. Prabhuram, R. Manoharan, J. Power Sources 74 (1998) 54.
[33] Z.L. Liu, X.Y. Ling, X.D. Su, J.Y. Lee, J. Phys. Chem. B 108 (2004) 8234.
[34] M. Bergelin, J.M. Feliu, M. Wasberg, Electrochim. Acta 44 (1997) 1069.
[35] B.E. Hayden, A.J. Murray, R. Parsons, D.J. Pegg, J. Electroanal. Chem. 409 (1996) 51.
[36] U. Koponen, T. Peltonen, M. Bergelin, T. Mennola, M. Valkiainen, J. Kaskimies, M. Wasberg, J. Power Sources 86 (2000) 261.
[37] J. Chen, B. Lim, E.P. Lee, Y. Xia, Nano Today 4 (2009) 81.
[38] N.M. Markovic, P.N. Ross Jr., Surf. Sci. Rep. 45 (2002) 117.
[39] G. Ertl, N. Neumann, K.M. Streit, Surf. Sci. 64 (1977) 393.
[40] K.J.J. Mayrhofer, M. Arenz, B.B. Blizanac, V. Stamenkovic, P.N. Ross, N.M. Markovic, Electrochim. Acta 50 (2005) 5144.
[41] M. Watanabe, S.J. Motoo, J. Electroanal. Chem. 60 (1975) 259.
[42] H.A. Gasteiger, N. Markovic, P.N. Ross Jr., E.J. Cairns, J. Electrochem. Soc. 141 (1994) 1795.
[43] G. Tremiliosi, H. Kim, W. Chrzanowski, A. Wieckowski, B. Grzybowska, P.J. Kulesza, J. Electroanal. Chem. 467 (1999) 143.
[44] J.C. Davies, B.E. Hayden, D.J. Pegg, Surf. Sci. 467 (2000) 118.
[45] J.B. Goodenough, A. Hamnett, R. Manoharan, B.J. Kennedy, S.A. Weeks, J. Electroanal. Chem. 240 (1988) 133.
[46] M. Krausa, W. Vielstich, J. Electroanal. Chem. 379 (1994) 307.
[47] T. Frelink, W. Visscher, J.A.R. Van veen, Langmuir 12 (1996) 3702.
[48] A. Vittadini, A. Selloni, F.P. Rotzinger, M. Gratzel, Phys. Rev. Lett. 82 (1998) 2954.
[49] M. Lazzeri, A. Vittadini, A. Selloni, Phys. Rev. B 63 (2001) 155409.
[50] C. Arrouvel, M. Digne, M. Breysse, H. Toulhoat, P. Raybaud, J. Catal. 222 (2004) 152.
[51] S.J. Tauster, S.C. Fung, R.L. Garten, J. Am. Chem. Soc. 100 (1978) 170.
[52] H.Q. Song, X.P. Qiu, F.S. Li, Electrochim. Acta 53 (2008) 3708.
[53] M. Hepel, I. Dela, T. Hepel, J. Luo, C.J. Zhong, Electrochim. Acta 52 (2007) 5529.